European Coordination for Accelerator Research and Development

PUBLICATION

A study of beam position diagnostics using beam-excited dipole modes in third harmonic superconducting accelerating cavities at a free-electron laser

Zhang, P (The University of Manchester / DESY / The Cockcroft Institute) *et al*

24 May 2013

The research leading to these results has received funding from the European Commission under the FP7 Research Infrastructures project EuCARD, grant agreement no. 227579.

This work is part of EuCARD Work Package **10: SC RF technology for higher intensity proton accelerators and higher energy electron linacs**.

The electronic version of this EuCARD Publication is available via the EuCARD web site <http://cern.ch/eucard> or on the CERN Document Server at the following URL : <http://cds.cern.ch/record/1550962

A study of beam position diagnostics using beam-excited dipole modes in third harmonic superconducting accelerating cavities at a free-electron laser

Pei Zhang,[1,2] Nicoleta Baboi,[2] Roger M. Jones,[1,3] Ian R. R. Shinton,[1,3] Thomas Flisgen,[4] and Hans-Walter Glock[4]

[1)] *School of Physics and Astronomy, The University of Manchester, M13 9PL Manchester, United Kingdom*

[2)] *Deutsches Elektronen-Synchrotron (DESY), 22607 Hamburg, Germany*

[3)] *The Cockcroft Institute, WA4 4AD Cheshire, United Kingdom*

[4)] *Institut für Allgemeine Elektrotechnik, Universität Rostock, 18051 Rostock, Germany*

We investigate the feasibility of beam position diagnostics using Higher Order Mode (HOM) signals excited by an electron beam in the third harmonic 3.9 GHz superconducting accelerating cavities at FLASH. After careful theoretical and experimental assessment of the HOM spectrum, three modal choices have been narrowed down to fulfill different diagnostics requirements. These are localized dipole beam-pipe modes, trapped cavity modes from the fifth dipole band and propagating modes from the first two dipole bands. These modes are treated with various data analysis techniques: modal identification, direct linear regression (DLR) and singular value decomposition (SVD). Promising options for beam diagnostics are found from all three modal choices. This constitutes the first prediction, subsequently confirmed by experiments, of trapped HOMs in third harmonic cavities, and also the first direct comparison of DLR and SVD in the analysis of HOM-based beam diagnostics.

PACS number: 29.27.Bd, 29.90.+r

Rev. Sci. Instrum. **83**, 085117 (2012), DOI: http://dx.doi.org/10.1063/1.4748517

I. INTRODUCTION

Wakefields excited by electron bunches in accelerating cavities may adversely affect the beam quality and in the worst case result in a beam-break-up instability[1]. It is important to ensure these fields are well suppressed by extracting energy through special couplers. Indeed, for the acceleration of high intensity particle beams, suppressing the wakefields in both superconducting[2] and normal conducting[3] cavities is a common requirement. On the other hand, since the transverse wakefields depend on the transverse offset of the excitation bunch, they can also be used for beam diagnostics inside the cavity without additional vacuum components. The principle of using higher order modes (HOM, components of wakefield) for beam diagnostics has been proved in the TESLA 1.3 GHz cavities[4–6]. We plan to apply this idea to the third harmonic 3.9 GHz cavities[7]. To achieve this, special electronics are required[8], and are currently under design. The modal spectrum of the 3.9 GHz cavity is much more complex and significantly different compared to its 1.3 GHz cavity counterpart. Therefore, a feasibility study prior to the development of the electronics is essential. It is this aspect that is focused on in this paper. More specifically, this paper is devoted to investigating the beam diagnostics with beam-excited dipole modes in the third harmonic superconducting accelerating cavities at the FLASH[9] facility at DESY.

Compared to the TESLA 1.3 GHz cavity[10], wakefields are significantly larger in the third harmonic 3.9 GHz cavity. Therefore it is important to minimize these fields by aligning the beam with respect to the electrical axis of the cavity. This relies on accurate beam position diagnostics inside each cavity. However, conventional diagnostics instrumentations such as beam position monitors (BPMs) fall short of providing this information directly. Energy radiated to the HOM couplers of the cavity is capable of providing this information along with dedicated electronics. Prior to developing electronics, it is essential to characterize the HOMs and understand their behavior relating to beam offset. For this purpose, HOM measurements, both with and without beam-excitations, were conducted[11–16]. Simulations of the cavities, both with and without couplers, were also performed using various techniques[11,17,18]. HOMs were extensively studied so as to search appropriate modes for diagnostics. Three modal choices have been narrowed down and their position dependencies on the beam are studied. Localized dipole beam-pipe modes and trapped cavity modes from the fifth dipole band are suitable for local position determination in each individual component (beam pipe or cavity). On the other hand, propagating modes from the first two dipole bands enable the beam position to be determined more precisely for an entire four-cavity module, due to their strong coupling to the beam. Thus coupled modes and trapped modes provide complementary information.

This section presents an overview of the FLASH facility and the third harmonic cavities, followed by a brief description of the principle of beam position diagnostics using dipole modes. Section II proceeds with the HOM measurements of the third harmonic cavities both with and without beam-excitation, together with eigenmode simulations. HOMs are identified and the inter-cavity coupling effects observed in measurements and simulations are described. Detailed studies of HOM dependence on the beam offset for various modes are described in Section III. Final remarks constitute Section IV. Several data analysis techniques are used throughout the paper: a Lorentzian fit, linear regression and singular value decomposition. A direct comparison of direct linear regression and singular value decomposition is presented for the first time in the study of HOM-based beam diagnostics. The potential for using these techniques to measure beam position is described. The relative

merits of each dipole band in these techniques are carefully elucidated with reference to experiments conducted at FLASH.

FLASH[9] is a free-electron laser facility at DESY providing electron bunches with high peak current to generate coherent light with unprecedented brilliance. It is also a test facility for various accelerator studies.

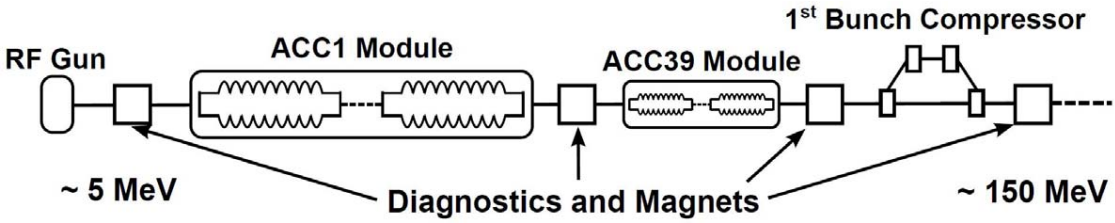

FIG. 1. Schematic of the injector section of FLASH facility.

Fig. 1 shows schematically the injector section of FLASH, which is relevant to our studies. The electron beam generated by a photoelectric gun is accelerated off-crest by eight superconducting 1.3 GHz TESLA cavities[10] in cryo-module ACC1 and compressed by the first magnetic chicane. The electron bunch typically has a length of approximately 2 mm prior to entering the first bunch compressor. The bunches are supplied with a sinusoidal accelerating field and consequently a curvature develops in the energy-phase plane. This leads to a long bunch tail and a reduction of peak current in the bunch compression. To linearize the RF field, harmonics of the fundamental accelerating frequency (1.3 GHz) of the main linac are added. At FLASH, third harmonic superconducting cavities operating at 3.9 GHz are used[19]. Four such cavities are placed in the ACC39 module.

The ACC39 module is composed of four cavities namely C1 through C4 (illustrated in Fig. 2). Each cavity is equipped with two higher order mode (HOM) couplers[20]. By extracting HOMs through these couplers, the wakefields are well-suppressed and their deleterious effects on the beam are minimized. Wakefields extracted from these couplers are guided by long cables to a HOM board rack outside the tunnel. After the module has been installed at FLASH, all the measurements were conducted from this rack, as will be discussed in Section II.

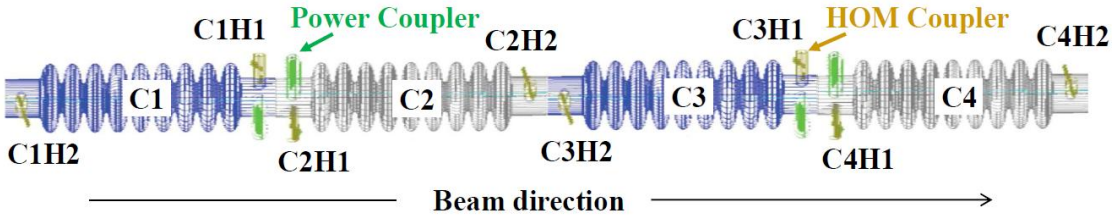

FIG. 2. Schematic of four cavities within ACC39 module.

By design[7], the 3.9 GHz cavity has two features in terms of wakefields compared to the 1.3 GHz cavity. Firstly, the wakefields in the 3.9 GHz cavity are larger as the iris radius is significantly smaller: 15 mm in the 3.9 GHz cavity compared to 35 mm in the 1.3 GHz cavity. From scaling considerations, transverse wakefields $W_\perp$ in the cavity grow as[21] $W_\perp \sim a^{-3}$, where a is the iris radius. Secondly, the HOM spectrum of the 3.9 GHz cavity is significantly more complex. The main reason for this is that, unlike the TESLA cavity case, the majority

of the modes are above the cutoff frequencies of the beam pipes. This allows most of the modes from each independent cavity to propagate through to adjacent cavities. In this case, most modes reach all eight HOM couplers. This facilitates the damping of HOMs to be distributed[7]. This gives rise to much more dense HOM spectra of the third harmonic cavities.

In a periodic structure with cylindrical symmetry, an ultra-relativistic particle of velocity c excites transverse wakefields $\mathbf{W}_\perp$. During normal operations, bunches are contained in the near-axis region. Thus $\mathbf{W}_\perp$ is dominated by dipole modes[21,22] as (when $s > 0$)

$$\mathbf{W}_\perp \simeq \left(\hat{r}cos\theta - \hat{\theta}sin\theta\right) r' c \sum_n^\infty \left(\frac{R}{Q}\right)_n sin\frac{\omega_n s}{c}, \tag{1}$$

where $\hat{r}$ and $\hat{\theta}$ are the unit vectors in r and θ directions. The transverse position of the excitation particle is denoted as (r', θ') where θ' has been set to 0 because of the cylindrical symmetry. $(R/Q)_n$ and $\omega_n/2\pi$ are the (R/Q)[22] and the frequency of each dipole eigenmode n. The $(\hat{r}cos\theta - \hat{\theta}sin\theta)$ term describes the polarization of the dipole mode in the transverse plane. There are two polarizations of each dipole mode perpendicular to each other. The dipole transverse wakefield is of particular interest, since it has a linear dependence on the excitation particle's offset r', regardless of the observation position. This enables the beam position within the cavity to be remotely determined by monitoring the beam-excited dipole modes [4–6].

II. ANALYSIS OF THE HOM SPECTRUM

In order to understand the HOM spectra of the third harmonic cavities, modal characterization is needed at all stages after the fabrication of the cavities. Therefore, HOM measurements both with and without beam-excitations were performed. The signals were measured from all eight HOM couplers. A representative selection of these signals is shown in this section.

A. Measurement of the transmission parameter S_{21}

To search for suitable modes for diagnostics, the transmission parameter S_{21} was measured along the entire four-cavity string (from C1H2 to C4H2), and then compared with the one measured from upstream and downstream couplers of each cavity within the cryo-module (see Fig. 3). Most HOMs couple to adjacent cavities through attached beam pipes. These are the peaks present in both the cavity C1 spectrum (blue) and the string spectrum (red). The usual discrete modes which are below the cutoff frequencies of the attached beam pipes can also be observed (peaks present only in C1 spectrum but absent from the string spectrum). The theoretical cutoff frequency of the beam pipe is 4.39 GHz for dipole TE_{11} modes, while the measurement shows an even lower value at approximately 4.25 GHz. Dipole beam-pipe modes at approximately 4.1 GHz are clearly visible in Fig. 3(a) as localized modes. In addition, some modes in the fifth dipole band at approximately 9.05 GHz are also non-propagating as shown in Fig. 3(b). Simulations were made to reveal the electromagnetic field distributions of these modes, and are discussed in next section.

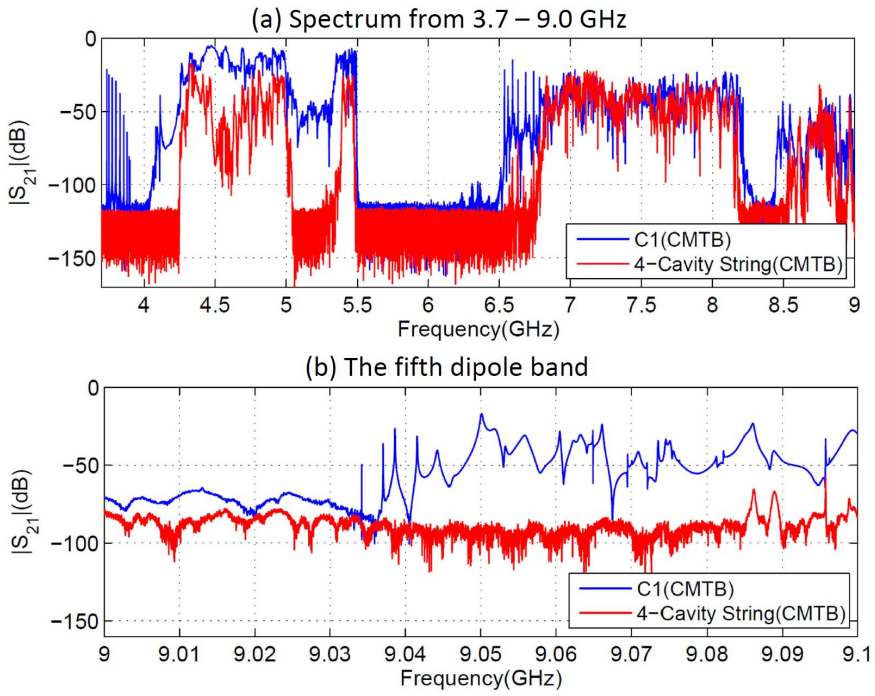

FIG. 3. Coupling effects amongst inter-connected cavities. The measurements were made at CMTB (Cryo-module Test Bench) at DESY.

B. Eigenmode simulations

An ideal third harmonic cavity without power coupler and HOM couplers was simulated with the Eigenmode Solver of CST Microwave Studio[18]. Dipole beam-pipe modes at approximately 4.1 GHz are observed as localized in the transmission measurements. The electric field of one of these modes is shown in Fig. 4(a). Electromagnetic energy mainly deposits in the beam pipes and the end-cells of the cavity, and is indeed trapped within both beam-pipe ends of the structure. The dipole character of the mode can also be seen in Fig. 4(a), where the field distribution is projected on the transverse plane in the middle of each end-cell. Fig. 4(b) shows the electric field of one mode in the first dipole band. The mode can couple to adjacent cavities through the attached beam pipes, and has a strong coupling to the beam represented by the large R/Q value. Some modes in the fifth dipole band are observed as trapped, which can be seen in Fig. 4(c) for one example. Compared with other trapped modes in this band, it has stronger coupling to the beam.

C. Measurement of the beam-excited HOM spectrum

The beam-excited HOM spectra were measured using a Tektronix Real-time Spectrum Analyzer (RSA)[23]. The schematic setup is shown in Fig. 5. HOM signals were taken from both HOM couplers of all four cavities at ACC39 HOM patch panel outside the FLASH tunnel. In order to protect the RSA, a 10 dB external attenuator was connected to each HOM coupler to reduce the power of the beam-excited signals radiated to the coupler. Since the RSA has only one input channel, a RF multiplexer was used to connect one coupler to it during each measurement. We were running FLASH with one bunch per beam pulse in a

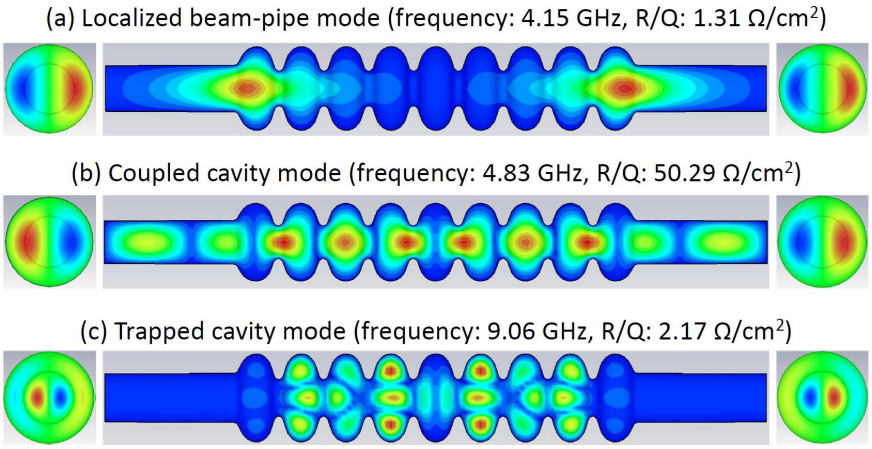

FIG. 4. Electric field distributions from eigenmode simulations of an ideal third harmonic cavity.

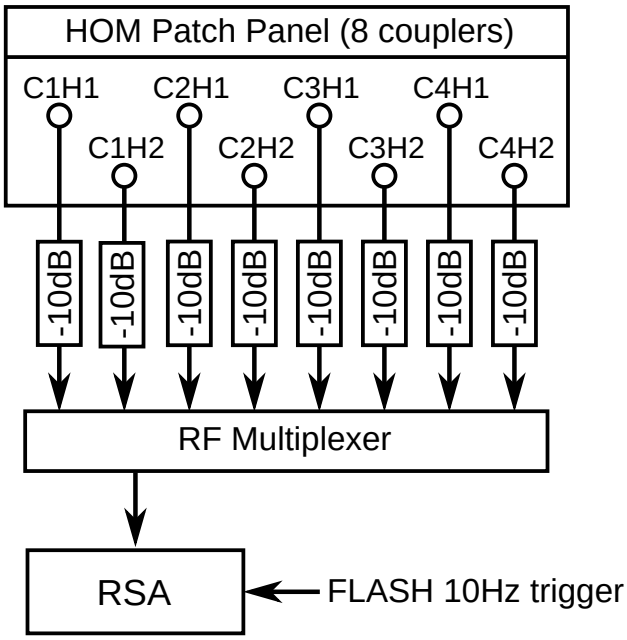

FIG. 5. Schematic setup for the beam-excited HOM spectra measurement. The 10 dB external attenuators have been removed during the measurement of the fifth dipole band.

repetition rate of 10 Hz. The bunch charge was 0.5 nC. The RSA was triggered by a 10 Hz RF signal delivered from the FLASH linac. A MATLAB[24] script was used to control the RF multiplexer and the RSA as well as the data recording to the local computer hard disk.

RSA has the capability to capture the HOM signal excited by a single bunch in a large bandwidth with a high frequency resolution. In our case, the acquisition bandwidth was set to 60 MHz with an acquisition length of 100 μs. A frequency step of 10 kHz and a resolution bandwidth of 22.5 kHz were used. The frequency span was set to 50 MHz. Starting from 4.025 GHz, the center frequency was raised in a step of 50 MHz. Thus the spectral ranges were consecutively recorded. Each 50 MHz slice of the spectrum corresponds to a single bunch excitation. Fig. 6(a)(b) shows the beam-excited spectrum of the localized dipole beam-pipe modes and the first two dipole bands. The spectrum of the fifth dipole band

is presented in Fig. 6(c) (without 10 dB external attenuator). The dependencies of these modes on the transverse beam offset were studied and are shown in the next section.

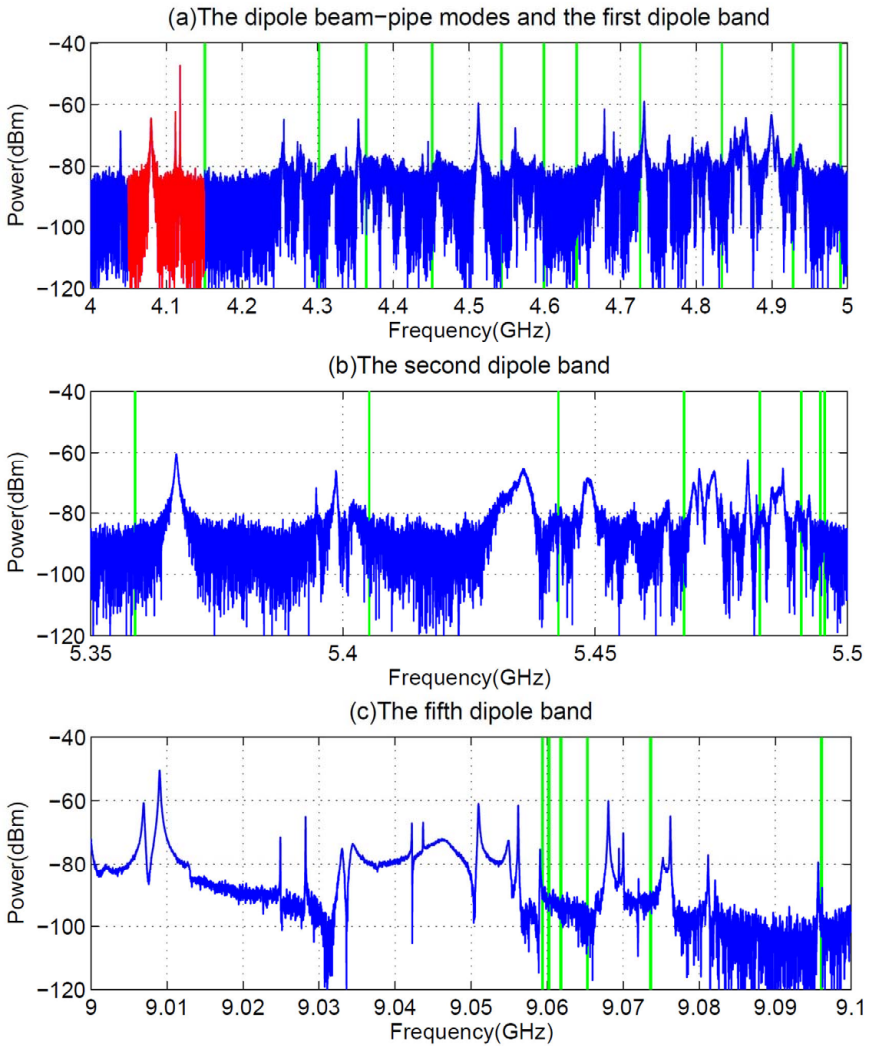

FIG. 6. Beam-excited spectra measured from HOM coupler C2H2 using RSA. The localized dipole beam-pipe modes are marked in red. The vertical lines denote dipole eigenmodes from simulations[18].

III. HOM DEPENDENCE ON THE BEAM OFFSET

After modal characterizations of the third harmonic cavities, experiments were conducted to find the correlation of dipole modes to the transverse beam position. Localized modes and coupled modes were studied. Various data analysis techniques were used: Lorentzian fit, linear regression and singular value decomposition. Linear dependencies are found and shown in this section. The direct linear regression method and the singular value decomposition method are compared in terms of prediction accuracy for both trapped and coupled modes.

A. Measurement setup

The schematic of the measurement setup is shown in Fig. 7. An electron bunch of approximately 0.5 nC is accelerated on-crest through ACC1 before entering the ACC39 module. Two steering magnets located upstream of ACC1 are used to produce horizontal and vertical offsets of the electron bunch in ACC39. Two beam position monitors (BPM-A and BPM-B) are used to record transverse beam positions before and after ACC39. Switching off the accelerating field in ACC39 and all quadrupoles close to ACC39, a straight line trajectory of the electron bunch is produced between those two BPMs. Therefore, the transverse offset of the electron bunch in each cavity can be determined by interpolating the readouts of the two BPMs.

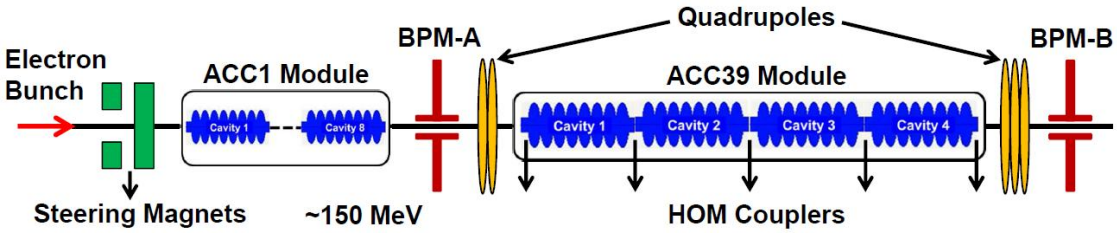

FIG. 7. Schematic of measurement setup for HOM dependence study (not to scale, cavities in ACC1 are approximately three times larger than those in ACC39).

For each beam position, along with HOM signals, nearby toroids, BPMs and currents of steering magnets are also recorded synchronously. The electron bunch is moved in two-dimensional (2D) cross manner and 2D grid manner. The steerers induce changes in beam offset and trajectory angle in ACC39. Due to technical difficulties to create trajectory angle in ACC39 independently and the contribution of the angle wakefield being much smaller than that of the offset wakefield[6], the angle is not considered in this study. The readings from BPM-A for these two scans are shown in Fig. 8. Position interpolations are applicable throughout this paper except the 2D cross scan (Fig. 8(a)) used for measuring beam-pipe modes. In this case, the quadrupoles between BPM-A and BPM-B were still on. One notices some tilt of the position readings during both scans. This is due to the coupling between x and y plane caused partially by the ACC1 module and partially by BPM-A itself. The quadrupoles can also contribute to the nonlinearity shown in Fig. 8(a).

B. Localized dipole beam-pipe modes

The spectra of two modes at approximately 4.1 GHz measured from C2H2 at ten different horizontal beam positions (diamonds in Fig. 8(a)) are shown in Fig. 9. According to the previous section, they are identified as dipole beam-pipe modes. The vertical position reading from BPM-A varied by ± 0.24 mm during the horizontal scan. Variations of the mode amplitude with respect to the horizontal beam position can be observed. The amplitudes have been normalized to the beam charge. The amplitudes do not reach zero, which might be due to an offset in the vertical direction during the horizontal scan. In addition, other sources such as fabrication errors and cell misalignment can also contribute.

Each mode corresponds to a resonant peak in the spectrum and is fit to the Lorentzian

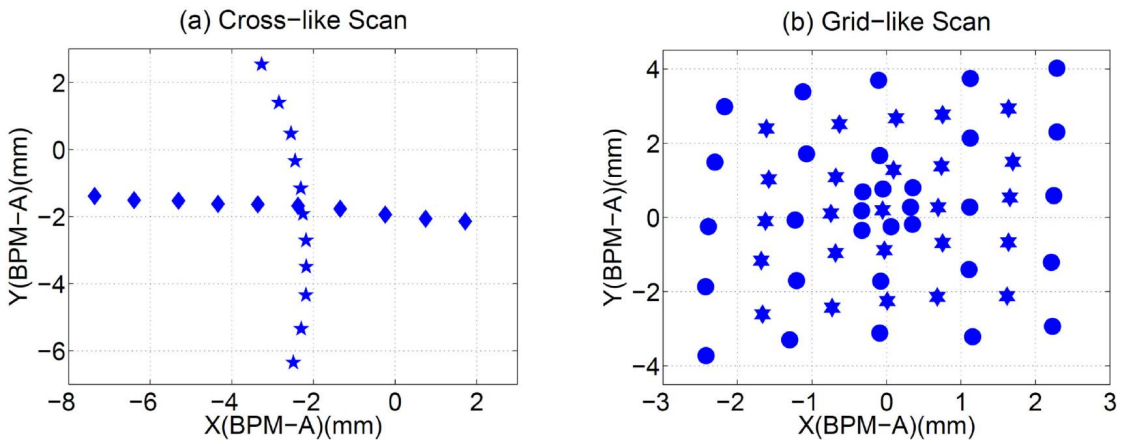

FIG. 8. Readings of BPM-A during beam scan.

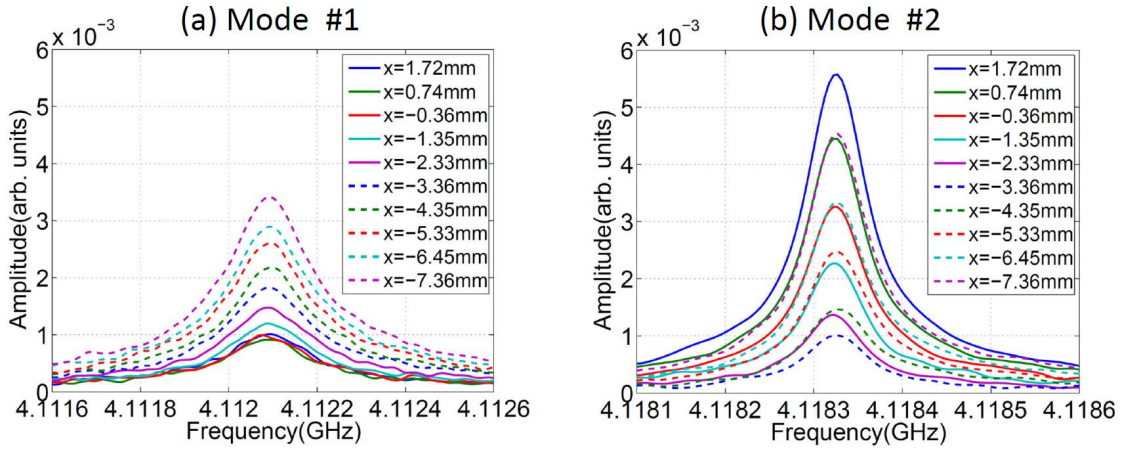

FIG. 9. Amplitude of dipole beam-pipe modes varies with transverse beam position read from BPM-A. The spectra were measured from HOM coupler C2H2.

distribution[25]:

$$y = \frac{y_0}{1 + (f - f_0)^2 / \Delta f^2}. \tag{2}$$

Here y_0 is the amplitude, f_0 is the center frequency and Δf is the half-width at half-amplitude. Fig. 10 shows the amplitude of each mode as a function of the transverse beam position read from BPM-A for both horizontal and vertical beam scans (Fig. 8(a)). A linear dependence of the mode amplitude on the transverse beam position can be observed, which indicates dipole-like behavior.

The polarization of each dipole beam-pipe mode is shown in Fig. 11 where the amplitude was measured in the 2D grid scan (Fig. 8(b)). Position interpolations from the two BPM readouts (BPM-A and BPM-B) are applied to get the transverse beam positions in the related beam pipe. These two modes are polarized perpendicularly, which indicates potential splitting of the mode degeneracy. This is also representative of dipole-like behavior. The symmetry of the ideal cylindrical structure is broken by the HOM couplers installed on the connecting beam pipes. This causes the frequency split of the two polarizations along with the inevitable manufacturing tolerances. There are three beam pipes inter-connecting

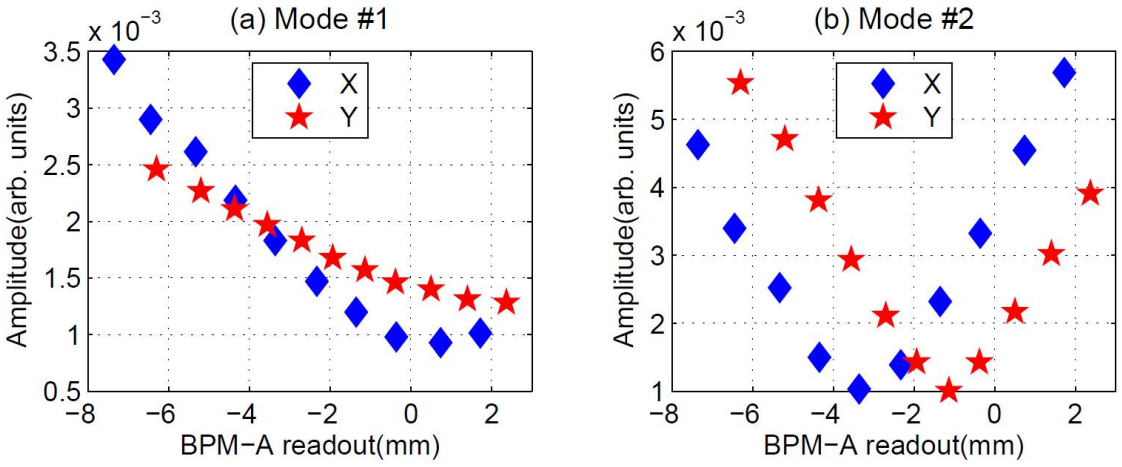

FIG. 10. Amplitude of dipole beam-pipe modes as a function of the transverse beam position read from BPM-A.

cavities in ACC39 (see Fig. 2), but clear polarizations can only be observed from the beam pipe connecting C2 and C3[16]. The power couplers installed on the other two beam pipes may account for this.

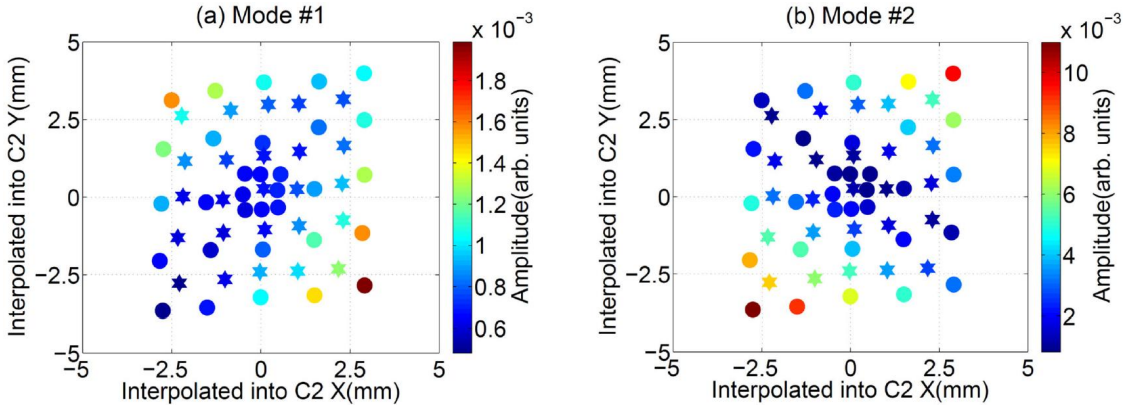

FIG. 11. Amplitude of dipole beam-pipe modes as a function of the transverse beam position interpolated into C2.

C. Trapped cavity modes in the fifth dipole band

As explained in Section II, trapped cavity modes exist in the fifth dipole band. By moving the beam horizontally, the variation of the amplitude of a mode at approximately 9.053 GHz can be clearly seen in Fig. 12(a). The vertical position in C1 varied by ±0.3 mm during this horizontal scan. Using a Lorentzian fit to obtain the amplitudes of the modes and plotting against horizontal beam positions interpolated from BPM readouts, the linear dependence can be clearly seen in Fig. 12(b) which indicates a dipole-like behavior.

In general, modes in the fifth dipole band have small amplitude, therefore a dedicated grid-like beam scan was conducted without the 10 dB external attenuators which were used

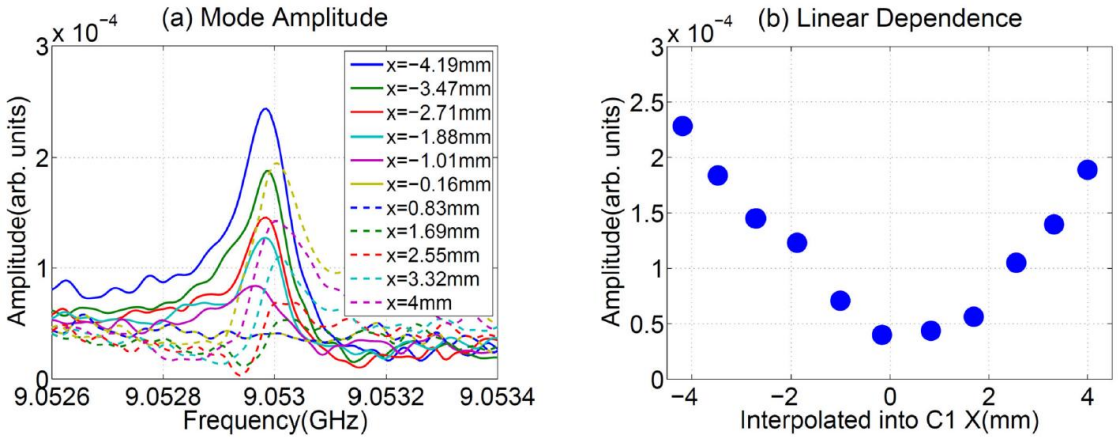

FIG. 12. Amplitudes of one dipole mode as a function of the transverse beam position interpolated into C1. The signals are measured from HOM coupler C1H1.

for other frequency bands. The interpolated beam positions are shown in Fig. 13(a). The amplitude of the same mode at approximately 9.053 GHz is again obtained by a Lorentzian fit for each beam position, and plotted in Fig. 13(b). The color denotes the amplitude magnitude. The polarization of this mode can be observed.

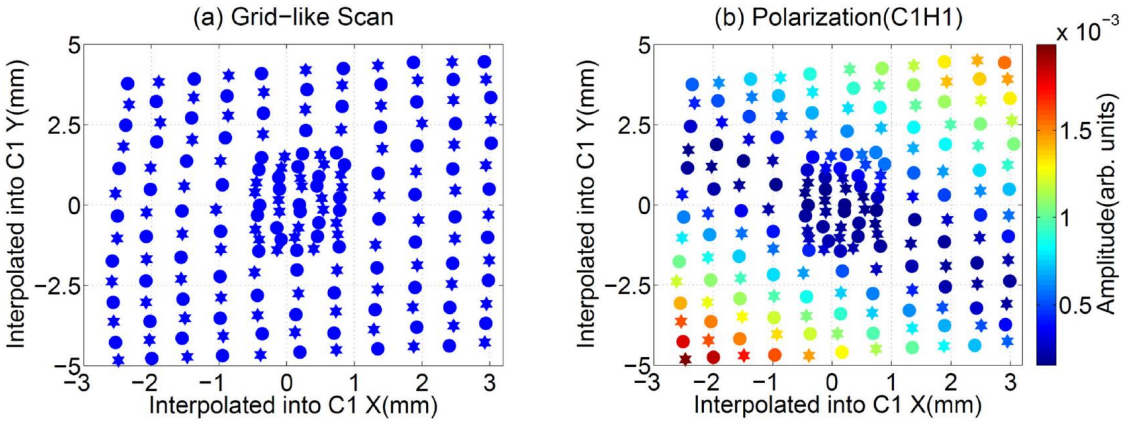

FIG. 13. (a) Grid-like beam scan. The positions are interpolated into C1. (b) Mode polarization (frequency: 9.053 GHz). The signals were measured from HOM coupler C1H1.

Spectra shown in Fig. 14 were recorded from all eight HOM couplers within the frequency range from 9.05 to 9.08 GHz. The spectrum from each HOM coupler of each cavity differs due to the fact that the HOM energy picked up by each coupler varies according to the detailed features of the individual couplers. As shown in Fig. 3(b), modes in this frequency range are trapped inside each cavity. Spectra within this bandwidth are therefore used for the following analysis.

1. direct linear regression (DLR)

Dipole modes have linear correlations to the transverse beam offset (Eq. 1). To extract beam position information from the dipole modes, a straightforward method is direct linear

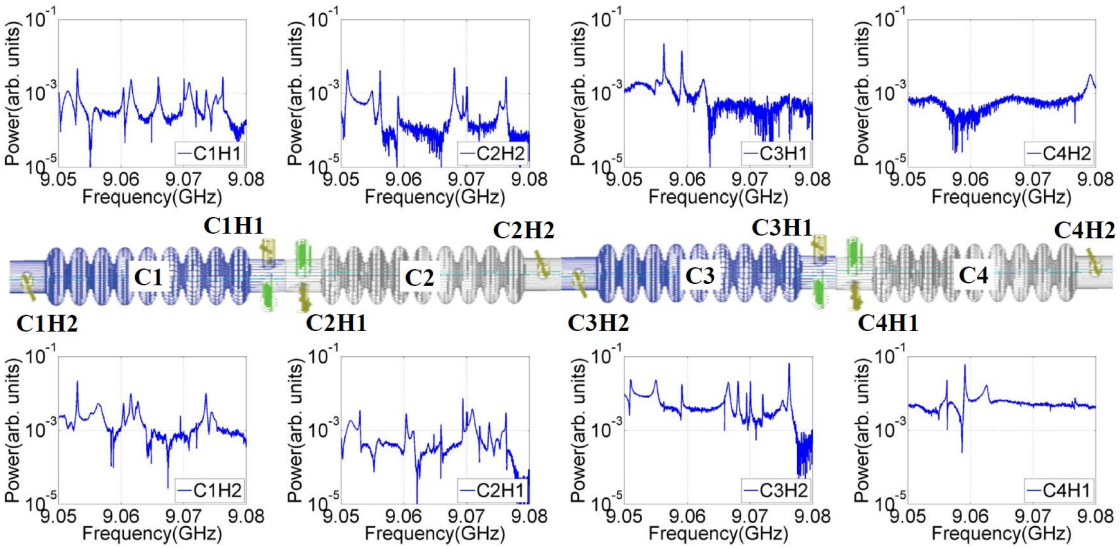

FIG. 14. Spectra measured from all eight HOM couplers of ACC39 module at one beam position.

regression (DLR),

$$A \cdot M = B. \tag{3}$$

In this equation, matrix A contains the magnitude of the HOM spectra (real and positive), B is the matrix of transverse beam position x and y interpolated from two BPM readouts. The angle of the beam trajectory x' and y' is not the subject of this study. M is the matrix of regression coefficients. Each row of A and B corresponds to one beam position. The intercept term for the regression is absorbed into A and M by adding one column of 1 in A and one row of coefficients in M. The matrix M is obtained by solving the linear system Eq. 3.

For the 2D grid beam scan, 184 samples (see Fig. 13(a)) are split equally into calibration samples (dots) and validation samples (hexagrams) in order to obtain full coverage in 2D space for both samples. They are denoted as (A^{cal}_{exp}, B^{cal}_{exp}) and (A^{val}_{exp}, B^{val}_{exp}).

The calibration samples are used to determine the matrix M, then the predictions of B can be obtained by

$$B^{cal}_{pre} = A^{cal}_{exp} \cdot M, \tag{4a}$$

$$B^{val}_{pre} = A^{val}_{exp} \cdot M, \tag{4b}$$

where B^{cal}_{pre} and B^{val}_{pre} are predictions of B for calibration and validation samples respectively. Applying DLR to the spectra measured from C1H1, we obtain the results for both samples. In Fig. 15(a), the prediction calculated by Eq. 4a and the measurement almost overlap, which proves the linear dependence of spectra on transverse beam offset. The linearity is further validated in Fig. 15(b) when using the calibration on the validation samples by Eq. 4b. To measure the consistency, the coefficient of determination r^2 is calculated and shown in the figure ($r^2 = 1$, perfect fit; $r^2 = 0$, poor fit)[26]. The prediction error is also calculated as

$$Prediction\ Error = B_{pre} - B_{exp}. \tag{5}$$

Fig. 16 shows the prediction error for calibration and validation samples by using DLR. The rms (root mean square) of the prediction errors (rms errors) for the validation samples are

0.1 mm (x) and 0.15 mm (y), which are comparable to those from the calibration samples. The calibration is robust.

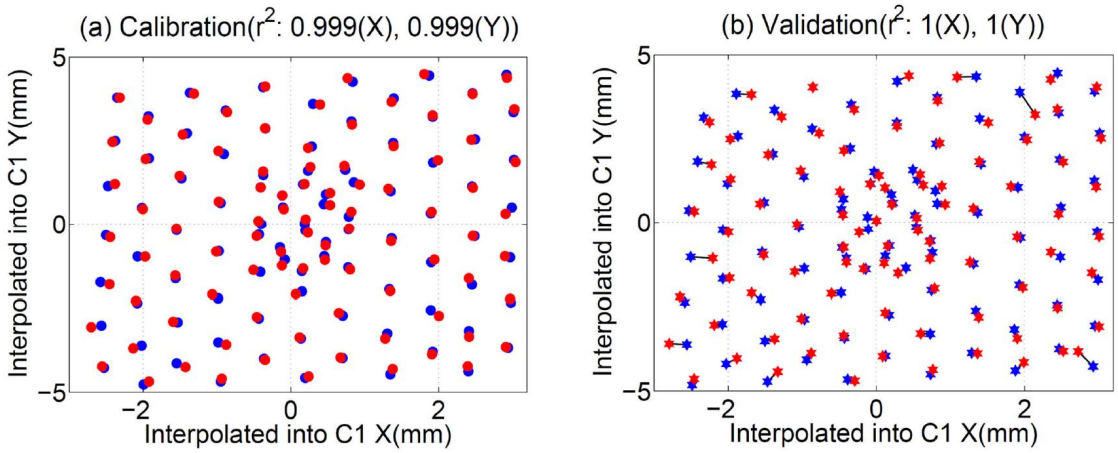

FIG. 15. Measurement (blue) and prediction (red) of the transverse beam position from calibration and validation samples (split as Fig. 13(a)). The method applied is DLR. Points connected with black lines belong to the same beam movement.

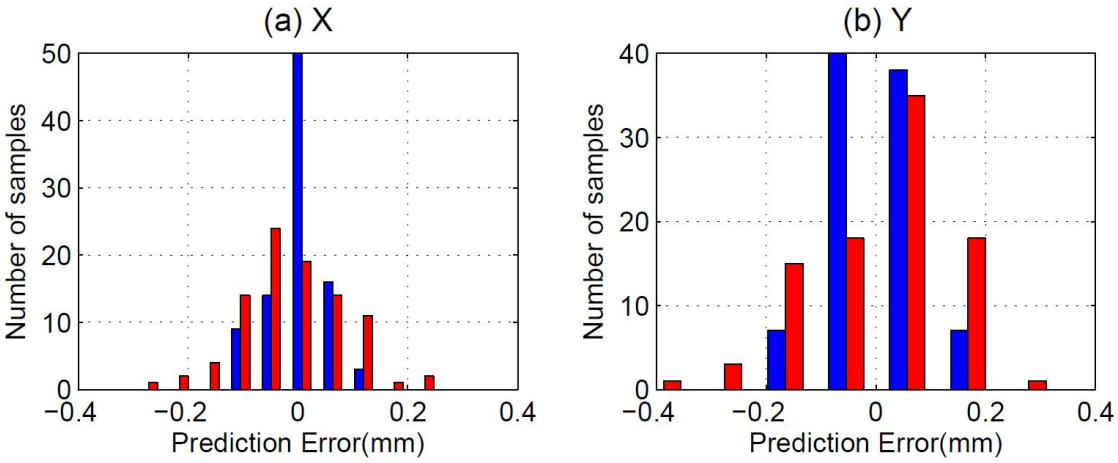

FIG. 16. Difference of measured and predicted transverse beam position from calibration (blue) and validation (red) samples. The method applied is DLR.

The algorithm used in solving the linear system (in the form of Eq. 3) is least squares, which is a standard method to solve linear regression problems. The method relies on minimizing the difference of prediction (B^{cal}_{pre}) and measurement (B^{cal}_{exp}) whilst modifying the elements of the matrix M. In our case, the size of matrix M is related to the number of sampling points, therefore a considerable number of unknown variables (in our case, 6242) needs to be determined. This is computationally expensive. It is also vulnerable to noise as all sampling points (the entire matrix A^{cal}_{exp}) are used in the regression. Moreover, even though it is not the case here, overfitting is always a potential problem unless the calibration samples are fairly large. To avoid this risk, it is better to reduce the system size from tens of thousands to several tens, and then apply linear regression on the reduced system. The method we used for this purpose is described in the following section.

2. *singular value decomposition (SVD)*

In order to find a small number of prominent components from the spectra matrix, a method known as *Singular Value Decomposition* (SVD) is used[27]. In general, SVD looks for the patterns of the matrix in terms of SVD modes without the knowledge of any physical parameters (like dipole mode frequency, quality factor, beam position, etc.). Those SVD modes are natural groupings of the spectra matrix, which are not clearly visible or explicitly defined in the matrix itself.

Applying SVD, the matrix A is decomposed into the product of three matrices,

$$A = U \cdot S \cdot V^T, \tag{6}$$

where V^T indicates the transpose of V. The columns of U and V^T are singular vectors of A, which form the bases of the decomposition. S is a diagonal matrix whose non-zero elements are known as singular values. Applying SVD on the calibration samples A^{cal}_{exp}, the singular value of each SVD mode is obtained and shown in Fig. 17(a). It can be seen that the first few SVD modes have relatively large singular values, in other words, they are the dominant patterns or natural groupings of matrix A^{cal}_{exp}. In this case, the first seventeen SVD modes are selected for the following analysis.

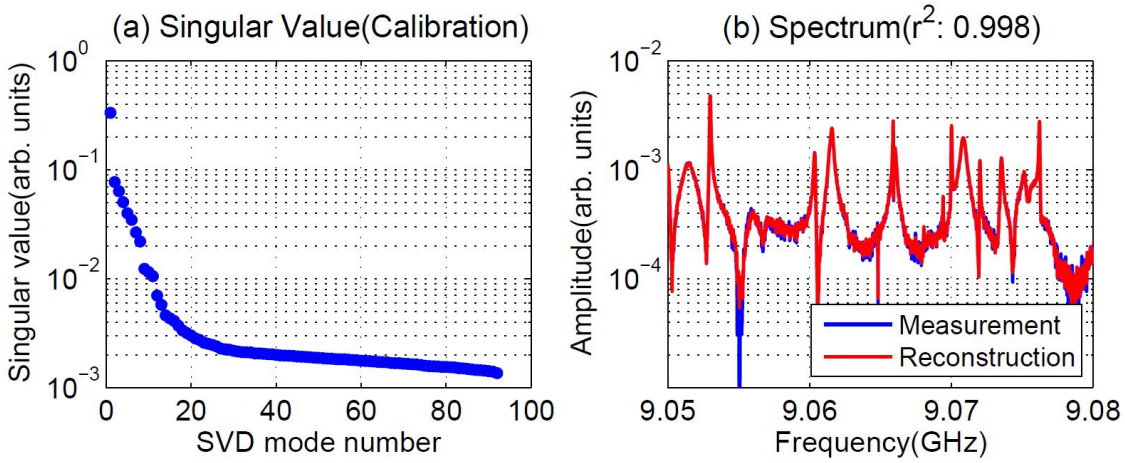

FIG. 17. (a) Singular values of SVD modes; (b) Reconstructed spectrum (red) from the first seventeen SVD modes compared with original spectrum (blue).

To examine how good the dominant SVD modes are to depict the original spectrum, one can use each of those SVD modes to produce a spectra matrix A^{cal}_i by

$$A^{cal}_i = U_i \cdot S_{ii} \cdot V^T_i, \tag{7}$$

where U_i is the i^{th} column of U, and V^T_i is the i^{th} row of V^T. S_{ii} denotes the i^{th} diagonal element of S. A^{cal}_i has the same size as A^{cal}_{exp}. Fig. 18 shows one spectrum for each of the first six A^{cal}_i. By combining the first seventeen SVD modes, the approximation A^{cal}_{reco} can be calculate by simply summing over the related A^{cal}_i by

$$A^{cal}_{reco} = \sum_{i=1}^{p} A^{cal}_i, \ p = 17. \tag{8}$$

A^{cal}_{reco} is plotted together with A^{cal}_{exp} in Fig. 17(b). The spectrum can be well represented by using only the first seventeen SVD modes.

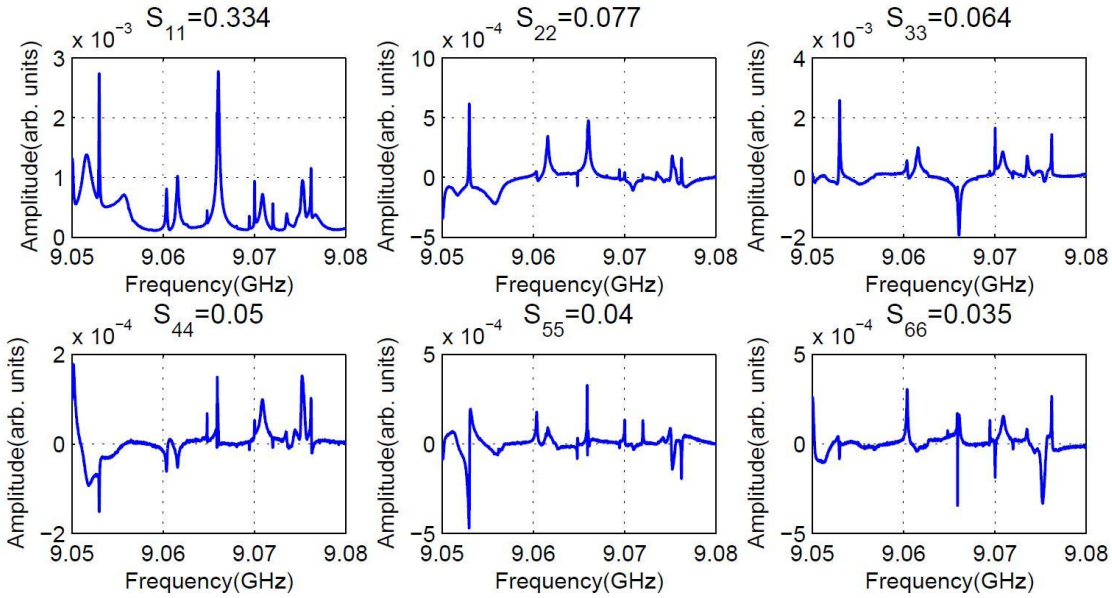

FIG. 18. Spectra reconstructed from each of the first six SVD modes.

Having the SVD base vectors from the decompositions of spectra matrix A^{cal}_{exp}, the amplitude of all SVD modes, $A^{cal}_{svd,full}$, can be obtained for each beam scan by

$$A^{cal}_{svd,full} = A^{cal}_{exp} \cdot V. \tag{9}$$

The first seventeen columns of the matrix $A^{cal}_{svd,full}$ constitute the matrix A^{cal}_{svd} along with one column of 1 representing the intercept term. The size of the matrix A^{cal}_{svd} is significantly smaller (18 columns, representing 17 SVD modes and one intercept term) compared to the original matrix A^{cal}_{exp} (6242 columns, representing 6241 sampling points and one intercept term). Replacing A^{cal}_{exp} by A^{cal}_{svd} in the regression (Eq. 3), the linear system composed by A^{cal}_{svd} and B^{cal}_{exp} is now over-determined, which has a well-known best solution. The prediction for the calibration samples B^{cal}_{pre} can be obtained using Eq. 4a by replacing A^{cal}_{exp} with A^{cal}_{svd}. The prediction for the validation samples has two steps: first, project A^{val}_{exp} onto the base vectors obtained from calibration samples to get the amplitude of the first seventeen SVD modes, A^{val}_{svd}, using Eq. 9 by replacing A^{cal}_{exp} with A^{val}_{exp}; second, using Eq. 4b to get the prediction B^{val}_{pre} by replacing A^{val}_{exp} with A^{val}_{svd}.

The contribution of combining the first p SVD modes to determine the transverse beam position x and y is measured by the rms errors as shown in Fig. 19. From Fig. 19(a), one can see that using the first seventeen SVD modes gives an optimal performance for the x plane. It is also a reasonable choice for the y plane (Fig. 19(b)) even though less SVD modes would be sufficient. This confirms, with Fig. 17, that the first few SVD modes contain most of the information.

Fig. 20 shows the HOM response from calibration and validation samples by using the first seventeen SVD modes to determine the transverse beam position x and y. The prediction errors remain small and comparable for calibration and validation samples as shown in Fig. 21. The rms error for the validation samples is 0.1 mm for x and 0.14 mm for y.

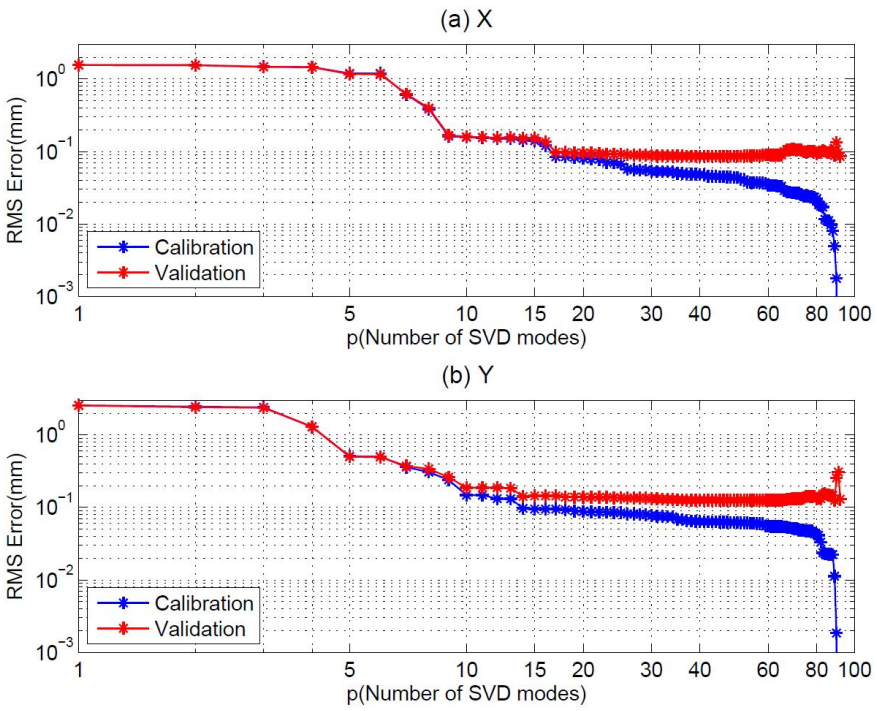

FIG. 19. Contribution of the first p SVD modes to determine the transverse beam position x and y.

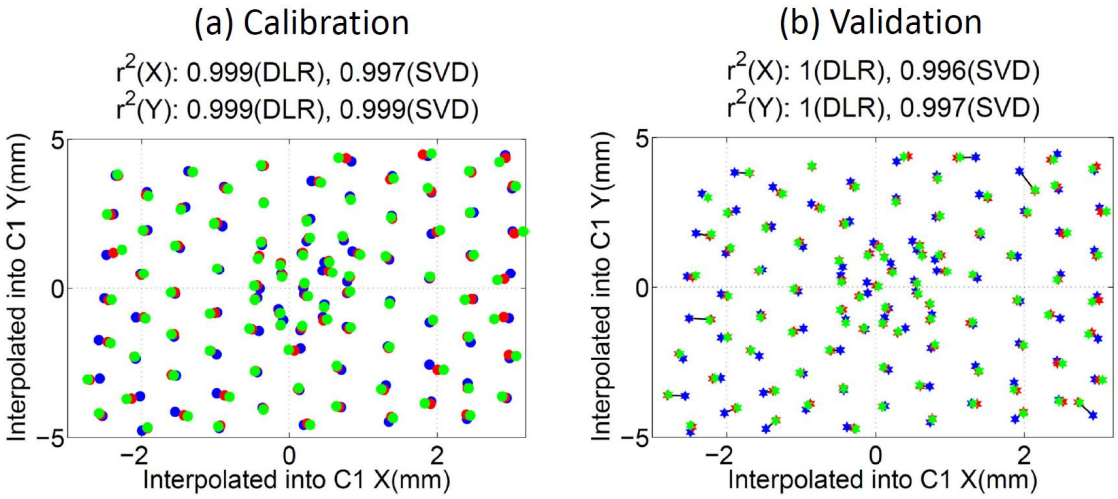

FIG. 20. Measurement (blue) and prediction of the transverse beam position from calibration and validation samples (split as Fig. 13(a)). The method applied is DLR (red) and SVD (green). Points connected with black lines belong to the same beam movement.

3. comparison of DLR and SVD

A direct comparison of DLR and SVD on the same samples (split as Fig. 13(a)) is shown in Fig. 20. The results are comparable. The comparisons of the prediction errors are listed in Table. I.

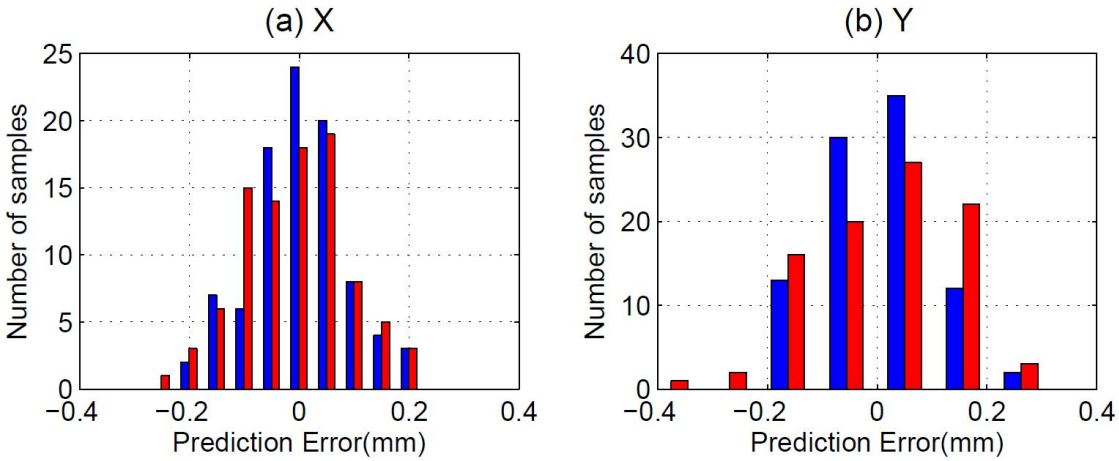

FIG. 21. Difference of measured and predicted transverse beam position from calibration (blue) and validation (red) samples. The method applied is SVD with the first seventeen SVD modes.

TABLE I. Comparison of rms errors of DLR and SVD for trapped cavity modes in 9.05–9.08 GHz and coupled cavity modes in 4.9–4.95 GHz.

	trapped modes		**coupled modes**	
RMS Error	$\boldsymbol{x}$(mm)	$\boldsymbol{y}$(mm)	$\boldsymbol{x}$(mm)	$\boldsymbol{y}$(mm)
Calib(DLR)	0.05	0.08	0.06	0.07
Calib(SVD)	0.08	0.09	0.20	0.09
Valid(DLR)	0.10	0.15	0.26	0.32
Valid(SVD)	0.10	0.14	0.24	0.28

In order to improve the prediction accuracy, multiple dipole modes in a narrow frequency band have been used for beam position determination rather than a single dipole mode (two polarizations,[6]). Then the number of SVD modes used for regression is determined by the magnitude of the singular values (Fig. 17(a)) and the prediction accuracy from the validation samples (Fig. 19). This turns out to be a larger number (17 SVD modes) than that in previous work[6] (6 SVD modes). This might be due to the fact that modes in the narrow frequency band have individual relationship to the beam scan.

Until now, our analysis is based on a specific sample split (Fig. 13(a)). To study the sample dependence, a technique named cross-validation is used[28]. The 182 samples are split randomly into calibration samples (129 samples, approximately 70% of the total samples) and validation samples (55 samples, the remaining 30%). Fig. 22 shows 8 different random splits.

Applying DLR and SVD on all 8 different splits, the responses of HOM spectra to the transverse beam positions represented by the rms errors are shown in Fig. 23. The variation amongst different validation samples remains small, which indicates that the HOM response does not rely on specific sample split. One can see that DLR performs slightly better than SVD, but SVD is far superior to DLR in terms of the computation time of the coefficient matrix M.

To extend the same analysis scheme to all other HOM couplers, spectra from 9.05 GHz to 9.08 GHz (see Fig. 14 for one beam position) are equally split as Fig. 13(a), then treated with DLR and SVD. The results are shown in Fig. 24. HOM spectra respond well for most

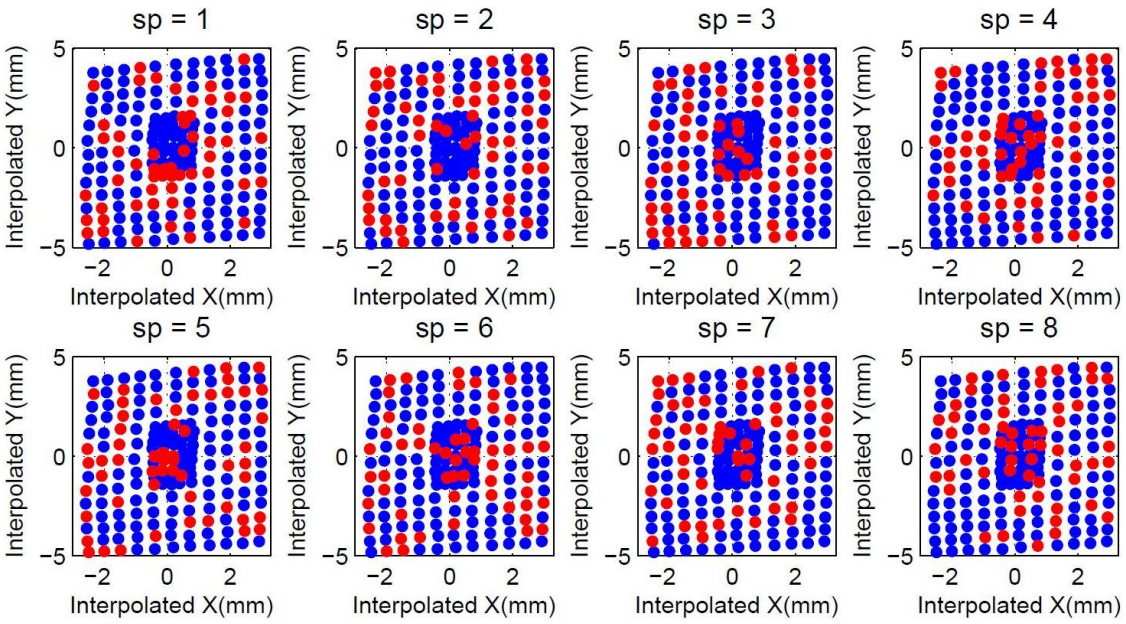

FIG. 22. Random splits of the total samples into calibration samples (blue) and validation samples (red). *sp* numbers the split. The beam positions are interpolated into C1.

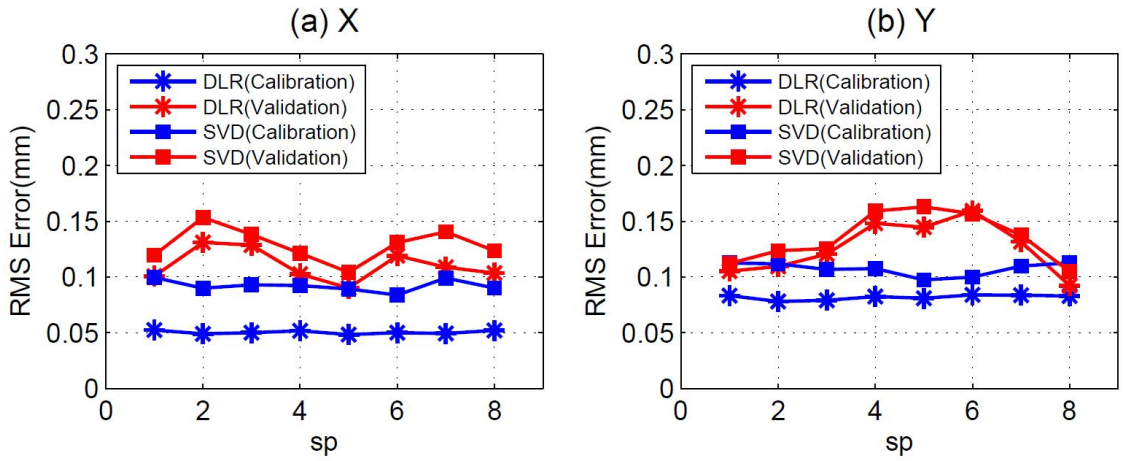

FIG. 23. RMS errors of calibration (blue) and validation (red) samples from 8 different splits (Fig. 22) by using DLR (asterisks) and SVD (squares).

couplers but differently to the beam scan for different HOM couplers. This comes from the different spectra and coupling behavior. It gives rise to special requirements of using HOMs for beam diagnostics[8], in particular a larger bandwidth is required to capture the frequency shifts among different HOM couplers.

4. discussion of the trapped cavity modes

According to simulations, some modes in the fifth dipole band are trapped cavity modes, meaning that electromagnetic (EM) energy mainly deposits inside each cavity (Section II)[14]

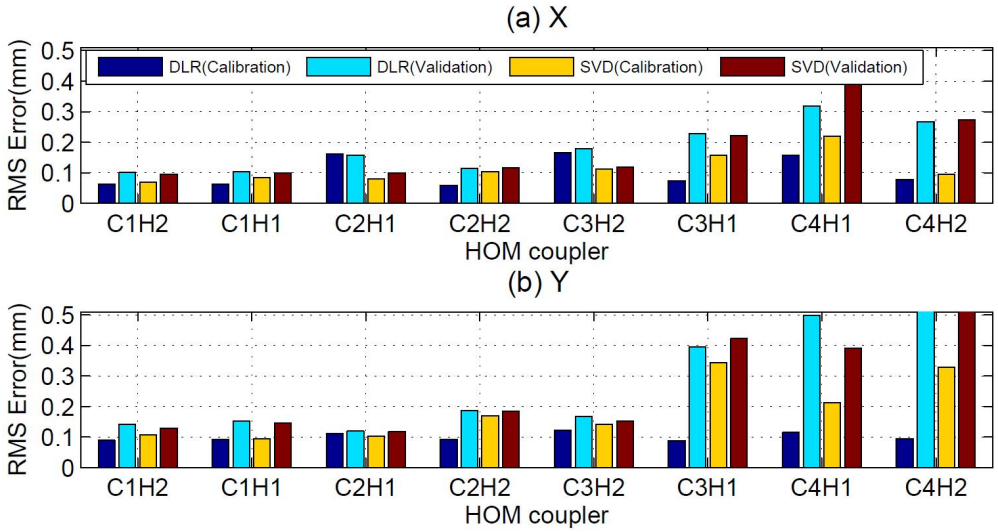

FIG. 24. RMS errors of all eight HOM couplers for spectra between 9.05 GHz and 9.08 GHz and split as Fig. 13(a).

and does not propagate to adjacent cavities through inter-connecting beam pipes. This fact enables the beam position to be determined locally within each cavity. This makes these trapped cavity modes attractive for beam diagnostics compared to the beam-pipe modes, where the EM fields are mainly in the beam pipes and end-cells, and to the first two dipole bands, where the modes couple among cavities (see the following section). However, modes in the fifth dipole band are located in an upper frequency range, and have small coupling to the beam (small R/Q values). The former will require careful electronics design and the latter will impact the position resolution in the electronics.

D. Coupled modes in the first two dipole bands

Both transmission and beam-based measurements have indicated a complex HOM spectrum in the third harmonic cavities, as described in Section. II. Most dipole modes are able to travel from cavity to cavity (see Fig. 3), among which are some strong coupling modes (high R/Q values) in the first two dipole bands. Unlike the localized beam-pipe modes and the trapped cavity modes, these multi-cavity modes enable the transverse beam position to be determined for an entire four-cavity module rather than local position inside each cavity or beam pipe. However, the 3.9 GHz four-cavity string is not significantly longer than one 1.3 GHz TESLA cavity (approximately 1.3 times), the position determined based-on the four-cavity module is still useful. Moreover, position diagnostics on these modes is relevant for beam alignment due to their strong coupling to the beam (high R/Q values)[15].

From simulations, the frequency range from 4.9 GHz to 4.95 GHz covers some strong coupling modes, therefore, the spectra within this 50 MHz bandwidth are used for the following analysis (the second dipole band spanning from 5.1 GHz to 5.5 GHz has been studied in[13]). The beam was moved in a grid manner and split into 32 calibration samples (dots) and 25 validation samples (hexagrams) as shown in Fig. 8(b). Then the positions read from BPM-A and BPM-B are interpolated into the center of the module.

As in the previous section, DLR and SVD are applied. The singular values of all SVD

modes decomposed from calibration samples are shown in Fig. 25(a). The first ten SVD modes have relatively large singular values, and therefore are used for the following analysis. The measured spectrum is compared with the reconstructed spectrum by using the first ten SVD modes in Fig. 25(b). They possess very good consistency, which indicates the representativeness of the first ten SVD modes in describing the entire signal. The SVD prediction errors for the validation samples are slightly better than those of DLR as shown in Table I.

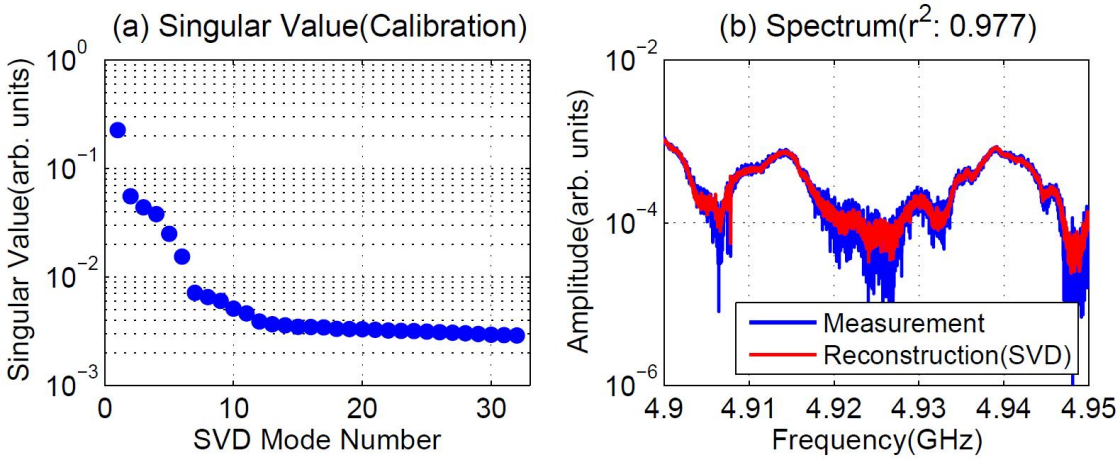

FIG. 25. (a) Singular values of SVD modes; (b) Reconstructed spectrum (red) from the first ten SVD modes compared with original spectrum (blue).

Compared to trapped cavity modes (Table I), coupled modes have larger prediction errors which is inconsistent with their stronger coupling to the beam (much higher R/Q). We believe it is coming from the fact that the signal over noise ratio is better for the trapped cavity modes due to the removal of the 10 dB external attenuator for each coupler during the data taking. This issue will be clarified after the measurements with the electronics.

IV. CONCLUSIONS

Beam-excited dipole modes in accelerating cavities can be used to determine beam position and also enables beam alignment to reduce the amplitude of beam-excited higher order modes (HOM). Dependencies of HOMs in third harmonic cavities on transverse beam positions have been observed for the first time. Beam-pipe modes, trapped and propagating cavity modes constitute three options for beam diagnostics. These have been narrowed down and studied by various data analysis techniques. Direct linear regression (DLR) and singular value decomposition (SVD) methods in particular, have been used to extract beam position from narrow bands of spectra. This is the first time that these two techniques have been compared directly in terms of performance and model complexity in the study of HOM-based beam diagnostics. Predicted beam positions indicate excellent agreement with direct measurements.

Beam-pipe modes and some cavity modes in the fifth dipole band are localized in segments of the module. This enables the beam position to be determined for individual component (beam pipe or cavity). We have identified modes and polarizations of two beam-pipe modes have been observed.

Cavity modes in the first two dipole bands propagate as shown by simulations and measurements. This enables the beam position to be determined for an entire four-cavity module. Good prediction accuracies are achieved with DLR and SVD. Due to their strong coupling to the beam, position diagnostics on these modes is relevant for beam alignment and for a reduction in the amplitude of the wakefield excited.

In this study, rms of the prediction errors are in the order of hundreds of μm for both propagating and trapped modes. They are mainly limited by the resolution of the real-time spectrum analyzer used for the measurement. Dedicated electronics for HOM-based beam diagnostics are under design. This will allow the phase information be added into the analysis along with the magnitude. The prediction accuracy is expected to be improved to tens of μm. We plan to test with the electronics and to investigate which of these three options fulfill our different diagnostics requirements.

ACKNOWLEDGMENTS

We would like to thank T. Khabibouline from FNAL for providing the data of module-based measurements at CMTB. We thank the FLASH crew at DESY lab for supporting the measurements. This work received support from the European Commission under the FP7 Research Infrastructures grant agreement No.227579. This work also received support from the Science and Technology Facilities Council (STFC) in UK.

REFERENCES

[1]K. Yokoya, "Cumulative Beam Breakup in Large Scale Linacs," DESY Report: 86-084, 1986.

[2]J.S. Sekutowicz, "HOM Damping and Power Extraction from Superconducting Cavities," in *Proceedings of LINAC 2006*, (Knoxville, Tennessee, USA), pp. 506–510, 2006.

[3]R.M. Jones, "Wake field Suppression in High Gradient Linacs for Lepton Linear Colliders," *Phys. Rev. ST Accel. Beams*, vol. 12, p. 104801, 2009.

[4]G. Devanz, M. Jablonka, C. Magne, O. Napoly, M. Huening and M. Wendt, "HOM Beam Coupling Measurements at the TESLA Test Facility (TTF)," in *Proceedings of EPAC2002*, (Paris, France), pp. 230–232, 2002.

[5]N. Baboi, G. Kreps, M. Wendt, G. Devanz, R. Paparella and O. Napoly, "Preliminary Study on HOM-Based Beam Alignment in the TESLA Test Facility," in *Proceedings of LINAC 2004*, (Lübeck, Germany), pp. 117–119, 2004.

[6]S. Molloy, J. Frisch, D. McCormick, J. May, M. Ross, T. Smith, N. Baboi, O. Hensler, L. Petrosyan, O. Napoly, R.C. Paparella, C. Simon, N. Eddy, S. Nagaitsev and M. Wendt, "High precision superconducting cavity diagnostics with higher order mode measurements," *Phys. Rev. ST Accel. Beams*, vol. 9, p. 112802, 2006.

[7]J. Sekutowicz, R. Wanzenberg, W.F.O. Müller and T. Weiland, "A Design of a 3^{rd} Harmonic Cavity for the TTF 2 Photoinjector," TESLA-FEL Report: 2002-05, 2002.

[8]N. Baboi, N. Eddy, T. Flisgen, H.-W. Glock, R.M. Jones, I.R.R. Shinton and P. Zhang, "Higher Order Modes for Beam Diagnostics in Third Harmonic 3.9 GHz Accelerating Modules," in *Proceedings of SRF2011*, (Chicago, USA), pp. 239–243, 2011.

[9]W. Ackermann *et al.*, "Operation of a free-electron laser from the extreme ultraviolet to the water window," *Nature Photonics*, vol. 1, pp. 336–342, 2007.

[10]J. Sekutowicz, *Multi-cell Superconducting Structures for High Energy e^+e^- Colliders and Free Electron Laser Linacs*. Warsaw, Poland: Warsaw University of Technology Publishing House, 2008.
[11]I.R.R. Shinton, N. Baboi, N. Eddy, T. Flisgen, H.W. Glock, R.M. Jones, N. Juntong, T.N. Khabiboulline, U. van Rienen and P. Zhang, "Higher Order Modes in Third Harmonic Cavities for XFEL/FLASH," in *Proceedings of IPAC'10*, (Kyoto, Japan), pp. 3007–3009, 2010.
[12]P. Zhang, N. Baboi, T. Flisgen, H.W. Glock, R.M. Jones, B. Lorbeer, U. van Rienen and I.R.R. Shinton, "First Beam Spectra of SC Third Harmonic Cavity at FLASH," in *Proceedings of Linear Accelerator Conference LINAC2010*, (Tsukuba, Japan), pp. 782–784, 2010.
[13]P. Zhang, N. Baboi, H. Ecklebe, T. Flisgen, H.W. Glock, R.M. Jones, B. Lorbeer and I.R.R. Shinton, "Beam-based HOM Study in Third Harmonic SC Cavities for Beam Alignment at FLASH," in *Proceedings of DIPAC2011*, (Hamburg, Germany), pp. 77–79, 2011.
[14]P. Zhang, N. Baboi, R.M. Jones and I.R.R. Shinton, "Study of Beam Diagnostics with Trapped Modes in Third Harmonic Superconducting Cavities at FLASH," in *Proceedings of IPAC2011*, (San Sebastián, Spain), pp. 2891–2893, 2011.
[15]P. Zhang, N. Baboi and R.M. Jones, "A Study of Beam Alignment Based on Coupling Modes in Third Harmonic Superconducting Cavities at FLASH," in *DITANET International Conference: Accelerator Instrumentation and Beam Diagnostics*, (Seville, Spain), 2011. e-prints: arXiv:1111.3479.
[16]P. Zhang, N. Baboi and R.M. Jones, "Higher order mode spectra and the dependence of localized dipole modes on the transverse beam position in third harmonic superconducting cavities at FLASH," DESY Report: 12-109, 2012.
[17]I.R.R. Shinton, R.M. Jones, Z. Li and P. Zhang, "Higher Order Modes in Coupled Cavities of the FLASH Module ACC39," in *Proceedings of IPAC2011*, (San Sebastián, Spain), pp. 2301–2303, 2011.
[18]P. Zhang, N. Baboi and R.M. Jones, "Eigenmode simulations of third harmonic superconducting accelerating cavities for FLASH and the European XFEL," DESY Report: 12-101, 2012.
[19]K. Flöttmann, T. Limberg and Ph. Piot, "Generation of Ultrashort Electron Bunches by Cancellation of Nonlinear Distortions in the Longitudinal Phase Space," TESLA-FEL Report: 2001-06, 2001.
[20]T. Khabibouline, I.G. Gonin and N. Solyak, "New HOM Coupler Design for 3.9 GHz Superconducting Cavities at FNAL," in *Proceedings of PAC07*, (Albuquerque, New Mexico, USA), pp. 2259–2261, 2007.
[21]K.L.F. Bane, "Wake Field Effects in a Linear Collider," SLAC Note: SLAC-PUB-4169, 1986.
[22]R. Wanzenberg, "Monopole, Dipole and Quadrupole Passbands of the TESLA 9-cell Cavity," TESLA Report: 2001-33, 2001.
[23]"Fundamentals of Real-Time Spectrum Analysis," Tektronix Application Note, 2010.
[24]MATLAB®. Ver. R2011b, The MathWorks Inc., USA, http://www.mathworks.com/.
[25]S.S.M. Wong, *Computational methods in physics and engineering*. Singapore: World Scientific Publishing Co., 1997.
[26]R.L. Ott and M. Longnecker, *An Introduction to Statistical Methods and Data Analysis*. Pacific Grove, California, USA: Duxbury Press, 2008.
[27]G.H. Golub and C.F. Van Loan, *Matrix Computations*. Baltimore, Maryland, USA: The

John Hopkins University Press, 1984.
[28]R. Kohavi, "A Study of Cross-Validation and Bootstrap for Accuracy Estimation and Model Selection," in *Proceedings of the 14th International Joint Conference on Artificial Intelligence*, vol. 2, (Montreal, Quebec, Canada), pp. 1137–1143, 1995.